

Scattering of α -particles and ${}^3\text{He}$ on ${}^{16}\text{O}$ nuclei and its excitation mechanism at energies near 50 MeV

N. Burtebayev^{*,†,||}, A. Duysebayev^{*}, B. A. Duysebayev^{*}, J. Burtebayeva^{*},
M. Nassurlla^{*,†}, B. Sadykov^{*}, T. K. Zholdybayev^{*}, N. Saduev[†], S. B. Sakuta[‡],
C. Spitaleri[§], B. G. Novatsky[‡], D. N. Stepanov[‡] and T. Kh. Sadykov^{†,¶}

^{*}*Institute of Nuclear Physics, Almaty, Kazakhstan*

[†]*Institute of Experimental and Theoretical Physics
of al-Farabi Kazakh National University, Almaty, Kazakhstan*

[‡]*National Research Center "Kurchatov Institute", Moscow, Russia*

[§]*National Institute of Nuclear Physics, Sezione di Catania, Catania, Italy*

[¶]*Institute of Physics and Technology, Almaty, Kazakhstan*

^{||}*nburtebayev@yandex.ru*

Received 21 October 2016

Revised 8 February 2017

Accepted 20 February 2017

Published 27 March 2017

Elastic and inelastic scattering of α -particles at 48.1 MeV and ${}^3\text{He}$ at 60 MeV on ${}^{16}\text{O}$ nuclei has been measured with excitation of states at 6.05 (0^+)–6.13 (3^-) MeV, 6.92 (2^+)–7.12 (1^-) MeV and 8.87 (2^-) MeV. The center-of-mass beam momenta are the same for these two strongly absorbed particles. Analysis of angular distributions was performed in the frameworks of the optical model, the coupled channels method and the Distorted Wave Born Approximation (DWBA). A good description of experimental data was obtained over the full angular range without taking into account the spin-orbit interaction and the cluster transfer mechanism with real potentials that have volume integrals of about 400 MeV fm³. Collective and microscopic models were used in the analysis of the inelastic scattering. The values of the octupole deformation lengths were extracted. It is shown that nuclear rainbow effects appear not only in the elastic, but also in the inelastic scattering with excitation of the 3^- state of ${}^{16}\text{O}$.

Keywords: Elastic and inelastic scattering; optical model; coupled channels; excitation mechanism.

PACS Number(s): 21.10.-k, 21.10.Pc, 21.10.Re, 24.45.De, 25.55.Ci

1. Introduction

The scattering of ${}^3\text{He}$ and α -particles on ${}^{16}\text{O}$ nuclei has been extensively studied over the past few decades, up to a beam energy of 150 MeV. The existing data can be divided into three sections. The first includes an energy range less than 15–20 MeV. Here, the scattering is determined mainly by the Coulomb interaction,

and differential cross sections are not sensitive to the inner area of nuclei. The primary goal of these experiments was to obtain information about the resonance energies, widths and the quantum characteristics of the composite states of the neon nucleus.^{1–8} At higher energies of the incident particles (20–40 MeV), the nuclear forces come into play. This leads to a change in the character of the scattering and in the angular distributions, a diffraction pattern is observed, as typical for the scattering on an absorbing sphere. Absorption leads to difficulties in obtaining information about the nucleus-nucleus potential at short distances, where densities of the colliding nuclei strongly overlap. This explains the ambiguity of the real part of the nuclear potential, which is determined from fits to the data in the optical model. However, for a number of light nuclei at very large angles corresponding to small impact parameters, the differential cross sections are to some extent sensitive to the inner nuclear area, resulting in anomalies which are unexplained by the standard optical model.^{9–11} And finally, at energies above 40 MeV, the scattering character of the ^3He and α -particle is changing again. This is due to the fact that nuclear forces are able to deflect these energetic particles only at an angle that does not exceed a certain limit θ_r , behind which there should be a shadow according to classical mechanics. This effect in the angular distributions is similar to the rainbow scattering in optics. According to quantum mechanics, near θ_r , a broad maximum must be present which is shifting toward smaller angles with increasing energy of the incident particles. At the same time, the diffraction structure can be observed only at angles smaller than θ_r , and at $\theta > \theta_r$, i.e. in the shadow area, there is an almost monotonic exponential fall-off.

As it was first shown in Refs. 12 and 13, for rainbow scattering, the angular dependence of the differential cross sections is very sensitive to the real part of the nuclear potential. That allows the removal of the discrete ambiguity in the optical model fitting.

The rainbow effects, manifested in the scattering of complex incident particles, are discussed in detail in a recent review.¹⁴ It is noted that for observations of the nuclear rainbow, it is necessary that the optical potential should be characterized by a strong attraction and a weak absorption simultaneously. In this case, the energy of the incoming particles should be large enough. Studies at the energies with a pronounced rainbow effect allow us not only to obtain information about the parameters of the nuclear potential, but also to explore the dependence of the effective nucleon–nucleon (NN)-interaction on the nuclear density and properties of the equation of state of the nuclear matter, using folding models.

But at energies where the rainbow effects occur, there are few experimental data. The scattering of α -particles on ^{16}O nuclei at energy higher than 40 MeV was investigated earlier at $E = 48.7$ and 54.1 MeV,¹⁵ 65 MeV,¹⁶ 69.5 MeV,¹⁷ 104 ,¹⁸ and 146 MeV.¹⁹ Only in Ref. 15, the measurements were carried out in the full angular range. In other cases, the measurements have been performed only in the forward hemisphere, and encounter the ambiguity of the determination of the nucleus-nucleus potential.

Scattering of the ${}^3\text{He}$ was studied much less. There are only three papers, where the measurements were performed at energies of 40.9 MeV,²⁰ 44 MeV²¹ and 60 MeV.²² It should be noted that the binding energy of the ${}^3\text{He}$ in light nuclei is of 10–15 MeV higher than that of α -particles. This should lead to a difference of their angular distributions, especially at large angles, due to the different contribution of the heavy cluster exchange mechanism $A(a, A)a$. Furthermore, for ${}^3\text{He}$, in contrast to the α -particle, the spin-orbit interaction can play a significant role.

Analysis of experimental data on the scattering of ${}^3\text{He}$ and α -particles by ${}^{16}\text{O}$ was previously performed only within the framework of the optical model. The phenomenological potentials have been found which give a good enough description of angular distributions. They correspond to the volume integral $J_V \sim 400 \text{ MeV fm}^3$ of the real part that is consistent with both the data of the global phenomenological analysis of the elastic scattering, performed for a wide range of nuclear targets and energies,^{23–25} and as well with the predictions of microscopic models. It has been shown that the inclusion of the spin-orbit interaction of ${}^3\text{He}$ in the calculation does not affect significantly the angular distributions.

The potentials obtained from microscopic models with single and double folding techniques (see, for example, Refs. 26–29), give a satisfactory description of elastic scattering for ${}^3\text{He}$ and α -particles in a wide energy range from 20 MeV to 150 MeV. Moreover, the normalizing factors for the potential depths are not strongly dependent on the energy and are close to unity, which implies that the NN interactions used are appropriate. Using different types of effective NN-interaction (M3Y, JLM), depending on the density, allowed authors to describe correctly the scattering data in the energy range where the nuclear rainbow effects are well manifested.

Inelastic scattering of α -particles with excitation of ${}^{16}\text{O}$ was studied previously only at energies of 40.5¹⁶ and 65 MeV.³⁰ Similar studies with ${}^3\text{He}$ beams at energies larger than 40 MeV have not been carried out. Research on light nuclei, including ${}^{16}\text{O}$, is convenient by the fact that the structure of low-lying states is well known. Furthermore, the level density is not high, so experiments with moderate resolution can be useful. Comparison of ${}^4\text{He}$ scattering to ${}^3\text{He}$ is very informative, especially for equal center-of-mass beam momenta. For inelastic scattering of ${}^4\text{He}$, only isoscalar transitions without changing the spin and isospin ($\Delta S = 0$, $\Delta T = 0$) are possible, while in ${}^3\text{He}$ scattering, both isoscalar and isovector transitions in the process going with the spin- and isospin-flip ($\Delta S = 1$, $\Delta T = 1$) are allowed. The objectives of this study are the investigation of elastic and inelastic scattering of ${}^3\text{He}$ and ${}^4\text{He}$ on ${}^{16}\text{O}$ at energies that permit rainbow scattering, with the same beam momentum, across a wide angular range. In addition, the role of channels coupling, excitation mechanism and two-step processes are studied for several transitions.

2. Experimental Setup and Results of Measurements

The measurements were performed at the isochronous cyclotron U-150M in the Institute of Nuclear Physics (Almaty, Kazakhstan) using extracted beams of ${}^3\text{He}$

and α -particles accelerated to energies of 48.1 MeV (α) and 60 MeV (^3He). A gas target was used in the experiment. It was a container of cylindrical shape, filled with natural oxygen (99.76% ^{16}O) to a pressure of about one atmosphere. The effective target thickness was 1–7 mg/cm², depending on the angle of measurement. The error in the thickness was not larger than 3%. The construction of the target was described in more detail in Ref. 31. The scattered ^3He and α -particles were detected and separated from the other charged reaction products using standard techniques (ΔE – E) with a telescope counters consisting of two silicon detectors with a thickness of 100 microns (ΔE) and 2 mm (E). Total energy resolution was about 500 keV and was determined by the energy spread of the beam, the target thickness and the angle of measurement. The uncertainty in our absolute differential cross sections is about 10%. Typical energy spectra of ^3He nuclei and α -particles are shown in Fig. 1. As it is seen, they are similar.

Apart from the elastic peak, two unresolved doublets are observed at 6.05 MeV (0^+)–6.13 MeV (3^-) and at 6.92 MeV (2^+)–7.12 MeV (1^-) as well as a broad structure at about 11.6 MeV, which includes several unresolved states. The anomalous parity state at 8.87 MeV (2^-) and a group of states in the region of excitation energy of $E_x = 13.3$ MeV are intensely excited in ^3He scattering, whereas in the scattering of α -particles they appear weakly.

The differential cross sections of elastic scattering were measured over an angular range of 10–170° (α -particles) and 10–150° (^3He) in the center-of-mass system. The measured angular distributions are shown in Fig. 2. It can be seen from the figure that both of their shapes are typical for rainbow scattering. There are broad maxima at angles of 50° (^3He) and $\sim 100^\circ$ (α -particles) and there is a well-defined diffraction structure at the smaller angles.

In the inelastic scattering with transitions to the states at 6.05 MeV (0^+)–6.13 MeV (3^-) and 8.87 MeV (2^-) (Fig. 2), this structure is also present, but not so strongly pronounced.

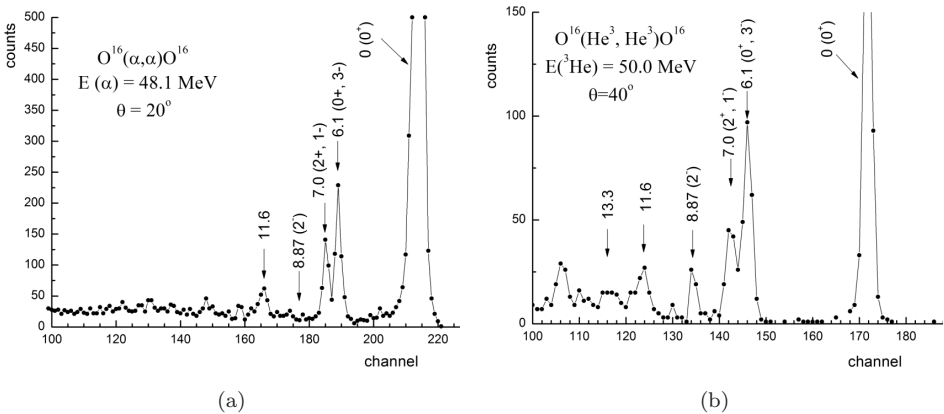


Fig. 1. The energy spectra of scattered ^3He (right) and α -particles (left), measured at the angles of 40° and 20°, respectively.

About the relative contribution of the 0^+ and 3^- states in the doublet observed at the excitation energy of 6.1 MeV, the following can be said. Firstly, as can be seen in Fig. 2, the cross sections of this group oscillate in phase with the elastic scattering. This corresponds, according to the Blair phase rule, to the predominant excitation of a state having opposite parity relative to the ground state. Secondly, this conclusion is confirmed by the analysis of the proton inelastic scattering,³² where the contribution of the 0^+ -state to the group of states with excitation energy of 6.1 MeV is not higher than 5%. Therefore, in our calculations, we take into account only excitation of the 3^- state.

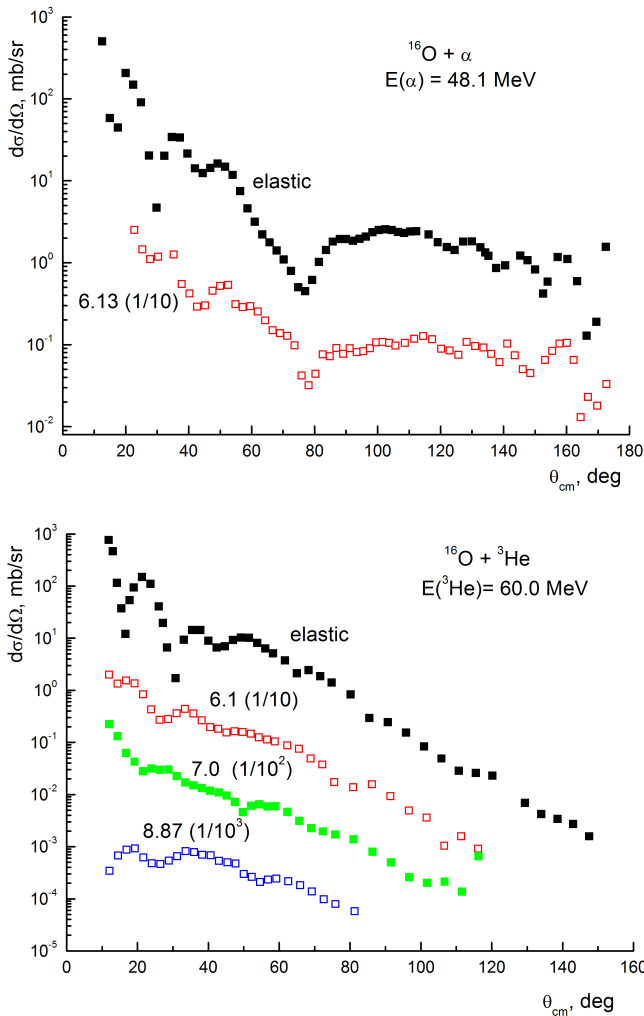


Fig. 2. The angular distributions of α -particles and ${}^3\text{He}$, scattered on ${}^{16}\text{O}$ nuclei with the transitions to the ground and excited states.

3. Analysis of Results and Discussion

3.1. Elastic scattering

The experimental data were compared to calculations within the frameworks of optical model, coupled reaction channel and the distorted wave methods. In all calculations, the phenomenological central potentials with volume or surface absorption were used in the form

$$U(r) = -Vf(r, R_V, a_V) - i \left(W_V - 4W_D a_I \frac{d}{dr} \right) f(r, R_I, a_I) + V_C(r), \quad (1)$$

where $f(r, R_i, a_i)$ is the Woods–Saxon form factor with geometric parameters of the radius $R_i = r_i A^{1/3}$ and diffuseness a_i ($i = V, I$):

$$f(r) = \left[1 + \exp \left(\frac{r - r_i A^{1/3}}{a_i} \right) \right]^{-1}. \quad (2)$$

V , W_V and W_D in (1) are the depths of the real and imaginary (with volume and surface absorption) potentials responsible for the nuclear interaction. V_C is Coulomb potential of a uniformly charged sphere with radius $R_C = r_C A^{1/3}$. In all calculations, the value of $r_C = 1.3$ fm was used.

The optimal potential parameters were found from the best description of the experimental angular distributions of elastic scattering in framework of the optical model by the least squares method. As starting potentials, we used potentials which have been found earlier from analysis for scattering of ^3He and α -particles on ^{14}N nuclei at energies close to ours.³³ Calculations were made using the SPI-GENOA program.³⁴ To reduce the ambiguity of the search, we tried not to go far from the recommended geometric parameters (r_i, a_i). The obtained potentials are given in Table 1.

The volume integrals of the real part of the potentials normalized to a pair of interacting particles of the incident particle and the target nucleus ($1/A_p A_t$) for systems $^{16}\text{O} + \alpha$ and $^{16}\text{O} + ^3\text{He}$ have the values of $J_V = 384.7$ and 404.6 MeV fm^3 , respectively. This is consistent with the predictions of microscopic models and to phenomenological global analysis of elastic scattering in a wide energy range.^{15,21,23} The comparison of the calculated cross sections with the experimental data is shown in Fig. 3.

It can be seen that the fitted curves (solid lines) reproduce well the structural features of the angular distributions of both α -particles and ^3He at the same

Table 1. The optical potential parameters obtained from the fitting to the elastic scattering data.

System	V (MeV)	r_V (fm)	a_V (fm)	J_V (MeV fm) ³	W_D (MeV)	r_I (fm)	a_I (fm)	J_W (MeV fm) ³
$^{16}\text{O} + \alpha$	129.3	1.225	0.725	385	8.00	1.56	0.69	74
$^{16}\text{O} + ^3\text{He}$	102.0	1.225	0.725	405	13.00	1.56	0.69	160

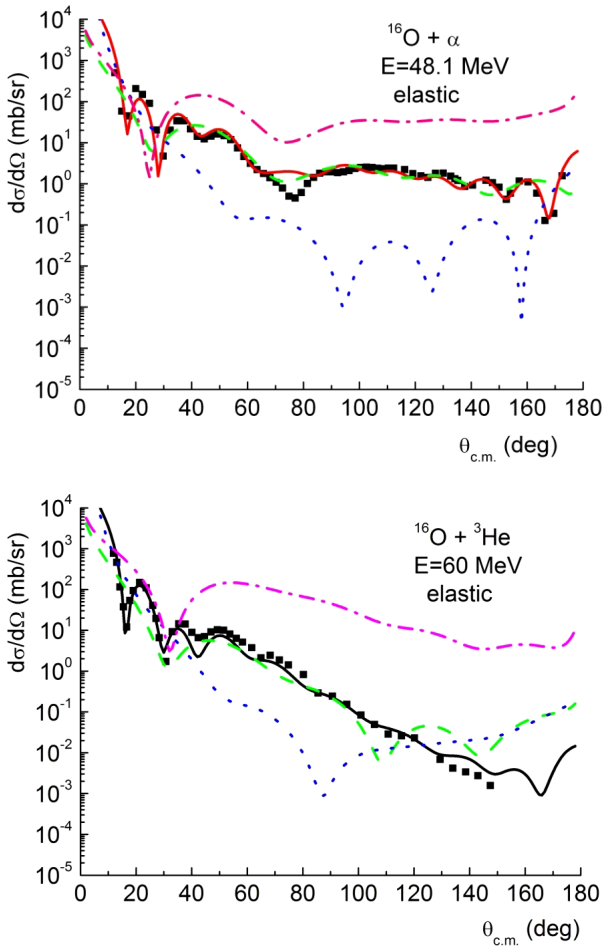


Fig. 3. The elastic scattering of α -particles and ${}^3\text{He}$ on ${}^{16}\text{O}$ nuclei. Dots-experiment. Solid curves-the optical model calculations with potentials presented in Table 1. The dashed and dotted curves show decomposition of the cross sections to the far- and the near-components, respectively. Dot-dashed curves-cross sections for the far component with the zero absorption ($W = 0$).

momentum transfers over the full angular range without taking into account the spin-orbit interaction and cluster exchange mechanisms.

Characteristic features of the measured angular distributions are the well-defined nuclear rainbow effects, manifested in the existence of Airy minima around the angles of 80° (for α -particles) and 40° (for ${}^3\text{He}$) and the observed unstructured fall-off with increasing scattering angles. The interpretation of these features is more transparent in the quasi-classical approach. In this case, the differential cross section at a given angle is determined by the contributions of the two trajectories. One trajectory corresponds to the scattering at the “near” edge of the nucleus and the other at the “far” edge with amplitudes $f_N(\theta)$ and $f_F(\theta)$, respectively.

Figure 3 shows the decomposition of the theoretical cross section for elastic scattering into near-side and far-side components. It can be seen that at large angles, the experimental cross sections are almost entirely reproduced by the far-side component $f_F(\theta)$, and at small angles, where the amplitudes $f_N(\theta)$ and $f_F(\theta)$ are comparable, large oscillations are observed due to their interference. The structure of the cross sections for the far-side component occurs due to the interference of the $l_>$ and $l_<$ trajectories of the deflection function for the scattering at the same angle. It manifests itself more clearly, if one turns off the absorption ($W = 0$). The cross sections calculated with $W = 0$ are shown in Fig. 3 by the dot-dashed curves. It is evident that in ${}^3\text{He}$ scattering, only one minimum at the angle about 30° is observed, while for α -particles, there are two minima (at $\sim 80^\circ$ and $\sim 30^\circ$) associated with the manifestation of the primary and secondary nuclear rainbows. Thus, in the elastic scattering of α -particles and ${}^3\text{He}$ on ${}^{16}\text{O}$ energies near 50 MeV, with the same momentum transfers, nuclear rainbow effects are well pronounced due to the refractive properties of the two nuclear potentials.

3.2. Inelastic scattering

The spins and parities of excited states in the inelastic scattering obey to certain selection rules. For transitions without changing the isotopic spin ($\Delta T = 0$), it can be written in the form

$$\mathbf{J} = \mathbf{L} + \mathbf{S}, \quad \Delta\pi = (-1)^l. \quad (3)$$

Here, \mathbf{J} , \mathbf{L} , \mathbf{S} are the total transferred angular momentum, orbital angular momentum and spin, $\Delta\pi$ represents a change of parity. The transferred momentum \mathbf{J} is defined by the vector relation $\mathbf{J}_f = \mathbf{J}_i + \mathbf{J}$, where \mathbf{J}_i and \mathbf{J}_f are the spins of the initial and final states of nuclei. From the selection rules, it follows that in the α -particles scattering, where always $\mathbf{S} = 0$, in the even-even nucleus, only the normal parity states (0^+ , 1^- , 2^+ , 3^- , etc.) can be excited, while in the scattering of ${}^3\text{He}$, where both values are $\mathbf{S} = 0$ and $\mathbf{S} = 1$ are possible, the abnormal parity states (0^- , 1^+ , 2^- , 3^+ , etc.) could be excited in the spin-flip processes.

3.2.1. Transition to the 3^- state at 6.13 MeV

The collective model. The excitation of the 3^- state in even-even nuclei is usually described in terms of the collective model. For ${}^{16}\text{O}$, it is known that this transition exhausts about 10% of the energy-weighted sum rule for octupole transitions.¹⁹ Calculations were performed by the coupled channels method using the FRESKO code³⁵ with the form factor responsible for the excitation of multipole order λ :

$$V_\lambda(r) = \frac{\delta_\lambda}{\sqrt{4\pi}} \frac{dU(r)}{dr}, \quad (4)$$

where δ_λ is the deformation length of multipolarity λ associated with the deformation parameter β_λ by the relation $\delta_\lambda = \beta_\lambda R$. For the 3^- state, a dynamic octupole

deformation ($\lambda = 3$) is assumed. In the calculations, we take into account the coupling of the elastic and inelastic scattering in both the forward and reverse directions.

The δ_λ is the only parameter, together with the optical potentials given in Table 1, needed to calculate the inelastic cross sections. For a better description of the elastic and inelastic scattering at large angles by the coupled channel methods, the depths of the imaginary part $W_D = 6.5$ MeV (α -particles) and $W_D = 12.0$ MeV (${}^3\text{He}$) have been slightly modified.

Comparisons of the cross sections, calculated for $\delta_3 = 0.8$ fm (α -particles) and $\delta_3 = 1.0$ fm (${}^3\text{He}$) (solid curves), with experimental data are shown in Fig. 4. In the case of α -particles scattering, the collective model gives a fairly good description of

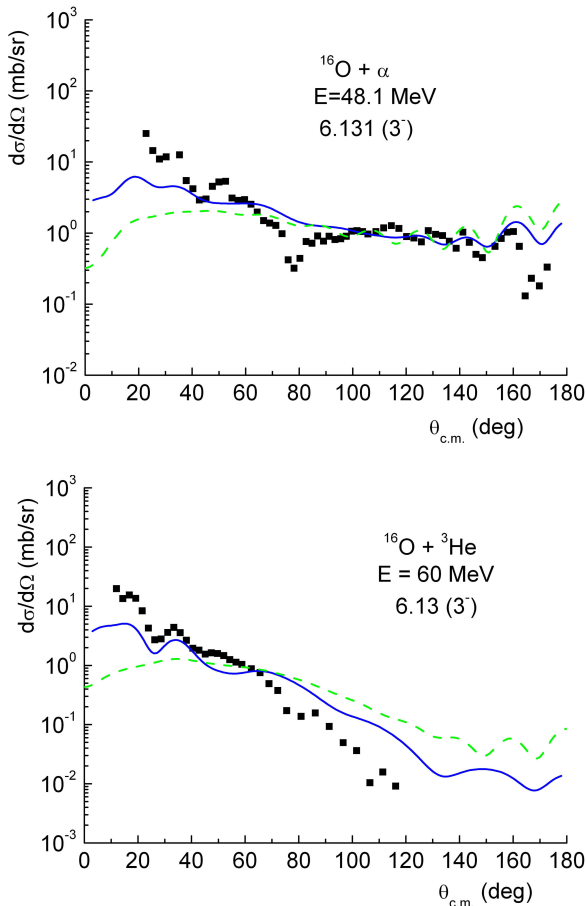


Fig. 4. The inelastic scattering of α -particles and ${}^3\text{He}$ by ${}^{16}\text{O}$ with the excitation of the 3^- state. Dots are experimental points. Curves are calculations with potentials given in Table 1. The solid and dashed curves are calculations in the framework of the collective and microscopic models, respectively.

the angular dependence, while for ${}^3\text{He}$, the computed cross sections at angles more than 80° are significantly higher than the experimental ones. Extracted deformation lengths (δ_3) correspond to the deformation parameters $\beta_3 = 0.259$ and 0.324 and to values of the reduced probabilities for octupole transitions ($B(E3) = 211$ and 330 in $e^2 \text{fm}^6$ units), respectively, calculated by the formula given in Ref. 35. The values obtained by us for β_3 and $B(E3)$ are substantially less than those given in the review paper³⁶ and in Ref. 37: $\beta_3 = 0.37\text{--}0.79$ and $B(E3) = 380\text{--}1740 e^2 \text{fm}^6$. However, this discrepancy can be explained by the normalization of the theoretical cross sections to the experiment. If you perform the normalization in the region of angles of $20\text{--}40^\circ$ (see Fig. 4), then our values will be in fairly good agreement with previous data.

Microscopic model. In the microscopic model, the inelastic scattering is described as the transition of nucleon from one orbit to another, due to the interaction of the incident particle and a valence nucleon of the target nucleus. The calculation in this model was conducted with potentials given in Table 1 using the DWBA method with a zero-range interaction, implemented in the program DWUCK4.³⁸ It was assumed that the excitation is caused by the transition of a single $p_{1/2}$ nucleon to the $d_{5/2}$ -shell. According to the selection rules (3), the transition to the 3^- state is determined by the amplitudes, characterized by quantum numbers (LSJ) = 303 (in α -particles scattering) and 303 as well as 313 (in ${}^3\text{He}$ scattering). In the present calculations, the radial dependence of the effective interaction is chosen in the form of the Yukawa potential with a range parameter $\mu = 1.0 \text{fm}^{-1}$

$$U_{\text{ST}}(r) = V_{\text{ST}} \frac{e^{-\mu r}}{\mu r}, \quad (5)$$

where V_{ST} is the interaction strength. The value of the cross section of inelastic scattering is proportional to the square of interaction strength, which is determined by fitting the computed cross section to the experimental data.

The one-particle wave function for the bound nucleon was found in the standard way using a Woods–Saxon potential with reduced radius of $r_0 = 1.25 \text{fm}$ and a diffuseness of $a = 0.65 \text{fm}$. Its depth was sought from the fitting to the binding energy.

The calculation results in the microscopic model for transitions to the 3^- state in the scattering of α -particles and ${}^3\text{He}$ with the effective interaction $V_{00} = 50 \text{MeV}$ are shown in Fig. 4. Even for the scattering of ${}^3\text{He}$, the transition cross sections is almost exclusively determined by the component (LSJ) = 303.

3.2.2. Transition to the 2^- state at 8.87 MeV

Microscopic model. Excitation of this state is described as a single-particle $p_{1/2} \rightarrow d_{5/2}$ promotion caused by the interaction of the incident particle (${}^3\text{He}$) and a single nucleon in the target. As in the previous case, the calculations were performed in DWBA with a zero-range interaction using the code DWUCK4. But in

this case, according to the selection rules, only the spin-flip transitions ($S = 1$) are possible. Thus, the 2^- state can be excited only by the amplitudes ($LSJT$) = 1120 and 3120. So, the study of the transitions makes it possible to get information about the strength of the interaction $V_{ST} = V_{10}$. The effective interaction included only the central part. Its radial dependence, as in the calculations for the 3^- state is defined by the relation (5) with parameter $\mu = 1 \text{ fm}^{-1}$. The one-particle wave function for the bound nucleon was found in the standard way using a Woods–Saxon potential with reduced radius of $r_0 = 1.25 \text{ fm}$ and a diffuseness of $a = 0.65 \text{ fm}$. Its depth was sought from the fitting to the binding energy.

The results of the calculation for the excitation of the 2^- state in ${}^3\text{He}$ scattering with $V_{10} = 12 \text{ MeV}$ are shown in Fig. 5 by solid and dashed curves. It can be seen, that the amplitude $LSJ = 312$ (dashed line in Fig. 5) contributes to the cross sections not more than 1% and cross sections are almost entirely determined by the transition with the transferred angular momentum $L = 1$. The shape of the angular distribution obtained with the parameter $\mu = 0.7 \text{ fm}^{-1}$ and the effective interaction $V_{10} = 6 \text{ MeV}$, as shown in the figure, differs little from the results of calculations with parameter $\mu = 1.0 \text{ fm}^{-1}$.

Two-step processes. As noted above, in the direct process, the 2^- state can be excited only by ${}^3\text{He}$ scattering via spin-flip. However, this state is still noticeable in the α -particles scattering and since spin-flip cannot occur simply for spin-zero particles, other reaction mechanisms must exist which may contribute to the ${}^3\text{He}$ scattering. These mechanisms can include (1) two-step processes, (2) compound-nucleus formation and (3) scattering induced by the noncentral interaction due to the tensor and spin-orbit forces.

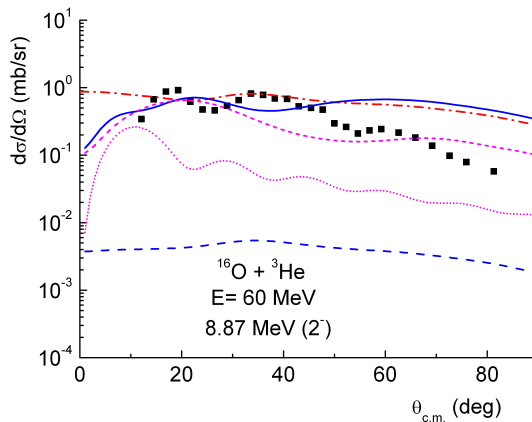


Fig. 5. The inelastic scattering of ${}^3\text{He}$ on ${}^{16}\text{O}$ nuclei with the excitation of the 2^- state. Dots—experiment. Curves—calculations with potentials given in Table 1. The solid and dashed curves correspond to the calculated cross sections using the microscopic model for the transferred $L = 1$ and $L = 3$, respectively. The dash–dot curve—calculation of the microscopic model with the parameter $\mu = 0.7 \text{ fm}^{-1}$. Dotted curves are the calculations in the assumption of a two-step mechanism for the transfer of the neutron (upper curve) and a proton (lower curve).

Table 2. Parameters of the potentials used for the calculations of cross sections for the ^3He scattering with excitation of the 2^- state by the coupled reaction channels method.

System	V (MeV)	r_V (fm)	a_V (fm)	W_D (MeV)	r_I (fm)	a_I (fm)
$^{15}\text{O} + \alpha$	129.3	1.225	0.725	8.00	1.56	0.69
$^{17}\text{F} + d$	102.3	1.225	0.725	13.00	1.56	0.69

To evaluate the possible contribution of two-step processes, coupled reaction channels calculations were performed for the most probable of them with the successive one-nucleon transfer. In these calculations as shown in Fig. 6, for the $^{15}\text{O} + \alpha$ and $^{17}\text{F} + d$ systems, potentials listed in Table 2 were used.

Neutron and proton transfers in both the directions were taken into account by the coupled reaction channels method. The corresponding diagrams are shown in Fig. 6. The calculated angular distributions (dotted curves) are compared with the experimental data in Fig. 5. The calculations were performed with the spectroscopic amplitudes (only for the ground states of the intermediate nuclei) equal to unity, which are close to theoretical values, as obtained in the translation invariant shell model.³⁹ The figure shows that in general, the absolute values and behavior of the angular distribution are reproduced well, although there is no maximum at the angle $\sim 40^\circ$ observed in the experiment. Calculations show (see Fig. 5) that the mechanism of sequential transfer of the neutron makes the main contribution. It is quite rough estimation, since the contributions of other possible channels were not taken into account. However, this result indicates that the contribution of the two-step process in the excitation of the 2^- state can play an important role.

3.2.3. Nuclear rainbow effects in inelastic scattering

Although nuclear rainbow effects were first observed and later investigated in detail in elastic scattering, it can be expected that they will also pronounce themselves in quasi-elastic processes (inelastic scattering, charge-exchange reaction and few-nucleon transfer reaction). Currently, there is increasing evidence in support of this concept.^{14,40} Generally speaking, due to the strong absorption in inelastic channels, nuclear rainbow effects should be less noticeable. However, if we compare the angular distributions of the elastic and inelastic scattering with the transitions to the

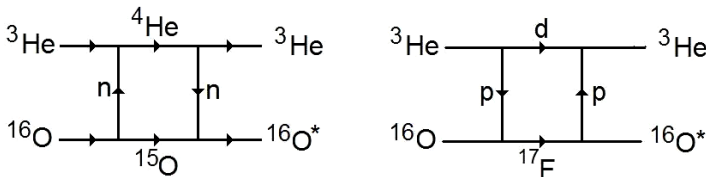


Fig. 6. The two-step processes with the successive neutron and proton transfer.

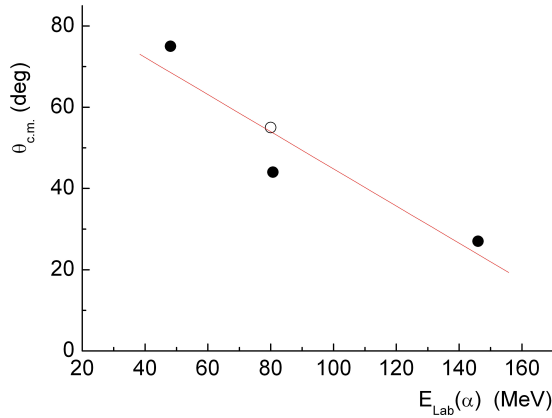


Fig. 7. Energy dependence of the Airy minima positions for inelastic scattering (excitation of 3^- state at 6.13 MeV). The solid circles at 80.7 and 146 MeV were taken from Ref. 40. The open circle is the position of the Airy minimum for the scattering of ${}^3\text{He}$ at 60 MeV (converted to an equivalent ${}^4\text{He}$ energy using $E({}^4\text{He}) = 4/3 E({}^3\text{He})$).

3^- state at $E_x = 6.13$ MeV (Figs. 3 and 4), which were measured in wide angular range, their remarkable similarity can be seen for the two beams.

In particular, in the scattering of α -particles and ${}^3\text{He}$ in both elastic and inelastic channels, the Airy minima are well marked at angles of about $\sim 80^\circ$ (α) and $\sim 50^\circ$ (${}^3\text{He}$). At forward angles, the diffractive structure is present while at the more backward angles, there is an almost monotonic exponential fall-off of differential cross sections. Moreover, it is known⁴¹ that with increasing energy of the incident particle, the rainbow angle is shifted by the law $\theta \sim 1/E$. In Fig. 7, the dependence of Airy minimum position on energy of α -particles is shown. The experimental results follow the $1/E$ rule.

Observation of nuclear rainbow effects in inelastic scattering suggests that the absorption is not so strong in the inelastic channel. This opens up the possibility of studying the interaction potential and transition form factors in quasi-elastic processes at small distances.

4. Summary

The angular distributions of elastic and inelastic scattering of α -particles (48.1 MeV) and ${}^3\text{He}$ (60 MeV) on ${}^{16}\text{O}$ nuclei were measured for transitions to the states 6.05 (0^+)–6.13 (3^-) MeV, 6.92 (2^+)–7.12 (1^-) MeV and 8.87 (2^-) MeV, at the same beam momentum. The optimal potential parameters were determined by fitting the calculated cross sections to the experimental data on the basis of the optical model. The obtained potentials were successfully used in the coupled channels and distorted wave calculations with a slight correction of the imaginary potential depths. A good description of elastic scattering of α -particles and ${}^3\text{He}$ over the full angular range has been obtained without taking into account the

spin-orbit interaction and heavy clusters transfer mechanisms. This indicates that the spin-orbit interaction and exchange mechanisms need not play a significant role.

Inelastic scattering was calculated in the framework of coupled channels and distorted wave methods. The calculations of differential cross sections for the transition into the 6.13 MeV (3^-) state were conducted on the basis of the collective and microscopic models.

The ^3He scattering with transition to the 8.87 MeV (2^-) state was calculated by the distorted waves method with a zero-range interaction, taking into account spin-flip. This calculation gives the closest values to the absolute experimental cross section, but poorly describes the details of the diffraction patterns with maxima at $\sim 20^\circ$, $\sim 40^\circ$ and $\sim 60^\circ$. The estimation of the possible contribution of two-step processes with a sequential transfer of the neutron or proton was made. It was shown that the two-step mechanisms can play a significant role in the excitation of the 2^- state.

In the inelastic scattering with the transition to the 3^- state, which measured a fairly wide angular range, the nuclear rainbow effects are clearly observed, suggesting that for this case absorption is not very large. This opens up the possibility in studying interaction and the transition form factors in the quasi-elastic processes at small distances.

Acknowledgments

The authors are grateful to Professor Peterson for valuable comments. The work was performed within the framework of the MES RK program - #0263/PSF "Study of the fundamental problems of modern physics as the basis of industrial-innovative development of Republic of Kazakhstan".

References

1. J. R. Cameron, *Phys. Rev.* **90** (1953) 839.
2. L. C. McDermott, K. W. Jones, H. Smotrigh and R. E. Benenson, *Phys. Rev.* **118** (1960) 175.
3. H. Röpke, K. P. Lieb and R. König, *Nucl. Phys. A* **97** (1967) 609.
4. W. E. Hunt, M. K. Mehta and R. H. Davis, *Phys. Rev.* **160** (1967) 782.
5. J. John, J. P. Aldridge and R. H. Davis, *Phys. Rev.* **181** (1969) 1455.
6. W. R. Ott and H. R. Weller, *Nucl. Phys. A* **179** (1972) 625.
7. J. H. Billen, *Phys. Rev. C* **20** (1979) 1648.
8. J. D. MacArthur, H. C. Evans, J. R. Lesile and H.-B. Mak, *Phys. Rev. C* **22** (1980) 356.
9. J. B. A. England, E. Casal, A. Garcia, T. Picazo, J. Aguilar and H. M. Sen Gupta, *Nucl. Phys. A* **284** (1977) 29.
10. B. I. Kuznetsov, P. E. Ovsyannikova and I. P. Chernov, *Yad. Fiz.* **15** (1972) 673; *Sov. J. Nucl. Phys.* **15** (1972) 377.
11. H. Oeschler, H. Schröter, H. Fuchs, L. Baum, G. Gaul, H. Lüdecke, R. Santo and R. Stock, *Phys. Rev. Lett.* **28** (1972) 694.
12. D. A. Goldberg and S. M. Smith, *Phys. Rev. Lett.* **29** (1972) 500.

13. D. A. Goldberg, S. M. Smith and G. F. Burdzyk, *Phys. Rev. C* **10** (1974) 1362.
14. D. T. Khoa, W. von Oertzen, H. G. Bohlen and S. Ohkubo, *J. Phys. G: Nucl. Part. Phys.* **34** (2007) R111.
15. H. Abele, H. J. Hauser, A. Körber, W. Leitner, R. Neu, H. Plappert, T. Rohwer, G. Staudt, M. Strasser, S. Welte, M. Walz, P. D. Eversheim and F. Hinterberger, *Z. Phys. A* **326** (1987) 373.
16. B. G. Harvey, E. J.-M. Rivet, A. Springer, J. R. Meriwether, W. B. Jones, J. H. Elliott and P. Darriulat, *Nucl. Phys.* **52** (1964) 465.
17. F. Michel, J. Albinski, P. Belery, Th. Delbar, Gh. Gregoire, B. Tasiaux and G. Reidemeister, *Phys. Rev. C* **28** (1983) 1904.
18. G. Hauser, R. Lohken, H. Rebel, G. Schatz, G. W. Schweimer and J. Specht, *Nucl. Phys. A* **128** (1969) 81.
19. K. T. Knöpfle, G. J. Wagner, H. Breuer, M. Rogge and C. Mayer-Böricke, *Phys. Rev. Lett.* **35** (1975) 779.
20. L. Alvarez and G. Palla, *J. Phys.(London)* **G8** (1982) 987.
21. R. Görgen, F. Hinterberger, R. Jahn, P. von Rossen and B. Schuller, *Nucl. Phys. A* **320** (1979) 296.
22. V. V. Adodin, N. T. Burtebaev and A. D. Duisebaev, *Yad. Fiz.* **55** (1992) 577; *Sov. J. Nucl. Phys.* **55** (1992) 319.
23. H.-J. Trost, A. Schwarz, U. Feindt, F. H. Heimlich, S. Heinzl, J. Hintze, F. Korber, R. Lekebusch, P. Lezoch, G. Mock, W. Paul, E. Roick, M. Wolfe, J. Worzeck and U. Strohmusch, *Nucl. Phys. A* **337** (1980) 377.
24. D. J. Pang, P. Roussel-Chomaz, H. Savajols, R. L. Varner and R. Wolski, *Phys. Rev. C* **79** (2009) 024615.
25. X.-W. Su and Y.-L. Han, *Int. J. Mod. Phys. E* **24** (2015) 1550092.
26. S. A. Khallaf, A. M. A. Amry and S. R. Mokhtar, *Phys. Rev. C* **56** (1997) 2093.
27. M. N. A. Abdullah, S. Hossain, M. S. I. Sarker, S. K. Das, A. S. B. Tariq, M. A. Uddin, A. K. Basak, S. Ali, H. M. Sen Gupta and F. B. Malik, *Eur. Phys. J. A* **18** (2003) 65.
28. D. T. Khoa, *Phys. Rev. C* **63** (2001) 034007.
29. H. Abele and G. Staudt, *Phys. Rev. C* **47** (1993) 742.
30. B. G. Harvey, J. R. Meriwether, J. Mahoney, A. Bussiere de Nercy and D. J. Horen, *Phys. Rev.* **146** (1966) 712.
31. A. D. Duisebayev *et al.*, *Izv. Akad. Nauk. Kaz. SSR, Ser. Fiz.-Mat.* **4** (1984) 73.
32. H. Ohnuma *et al.*, *Nucl. Phys. A* **514** (1990) 273.
33. N. Burtebayev, A. Duisebayev, B. A. Duisebayev, M. Nassurilla, S. K. Sakhiev, B. M. Sadykov, S. B. Sakuta, T. K. Zholdybayev, S. Kliczewski, R. Siudak and M. Wolińska-Cichočka, *Acta. Phys. Pol.* **47** (2016) 2017.
34. F. Perey, SPI-GENOA: An optical model search code (unpublished).
35. I. J. Thompson, *Comput. Phys. Rep.* **7** (1988) 167, available at: <http://www.fresco.org.uk/>.
36. T. Kibedy and R. M. Spear, *At. Data Nucl. Data Tables* **80** (2014) 112.
37. D. R. Tilley, H. R. Weller and C. M. Cheves, *Nucl. Phys. A* **564** (1993) 1.
38. P. D. Kunz, *Computer program DWUCK4. Zero range distorted wave Born approximation* (unpublished).
39. O. F. Nemets, V. G. Neudachin, A. T. Rudchik, Yu. F. Smirnov and Yu. M. Tchuvils'ky, *Nuclear Associations in Atomic Nuclei and Many-nucleon Transfer Reactions* (Naukova Dumka, Kiev, 1988).
40. H. Hirabayashi and S. Ohkubo, *Phys. Rev. C* **88** (2013) 014314.
41. J. Knoll and R. Schaeffer, *Ann. Phys.* **97** (1976) 307.